# Supporting information for Anisotropic Electron Transport Limits Performance in $Bi_2WO_6$ Photoanodes

Benjamin Moss,[a]* Haonan Le,[a] Sacha Corby,[a] Kazuki Morita,[b] Shababa Selim,[a] Carlos Sotelo-Vazquez,[c] Yunuo Chen,[a] Alexander Borthwick,[a] Anna Wilson,[a] Chris Blackman,[c] James R. Durrant,[a] Aron Walsh[b,d] and Andreas Kafizas,[a,e]*

[a]*Department of Chemistry, Molecular Science Research Hub, Imperial College London, White City Campus, London, W12 0BZ, U.K.*

[b]*Department of Materials, Imperial College London, Exhibition Road, London SW7 2AZ, U.K.*

[c]*Department of Chemistry, University College London, 20 Gordon Street, London, WC1H 0AJ, U.K.*

[d]*Department of Materials Science and Engineering, Yonsei University, Seoul 03722, South Korea*

[e]*Grantham Institute for Climate Change, Imperial College London, South Kensington, London, SW7 2AZ, U.K.*

**corresponding authors: b.moss14@imperial.ac.uk and a.kafizas@imperial.ac.uk*

**S0 XRD**

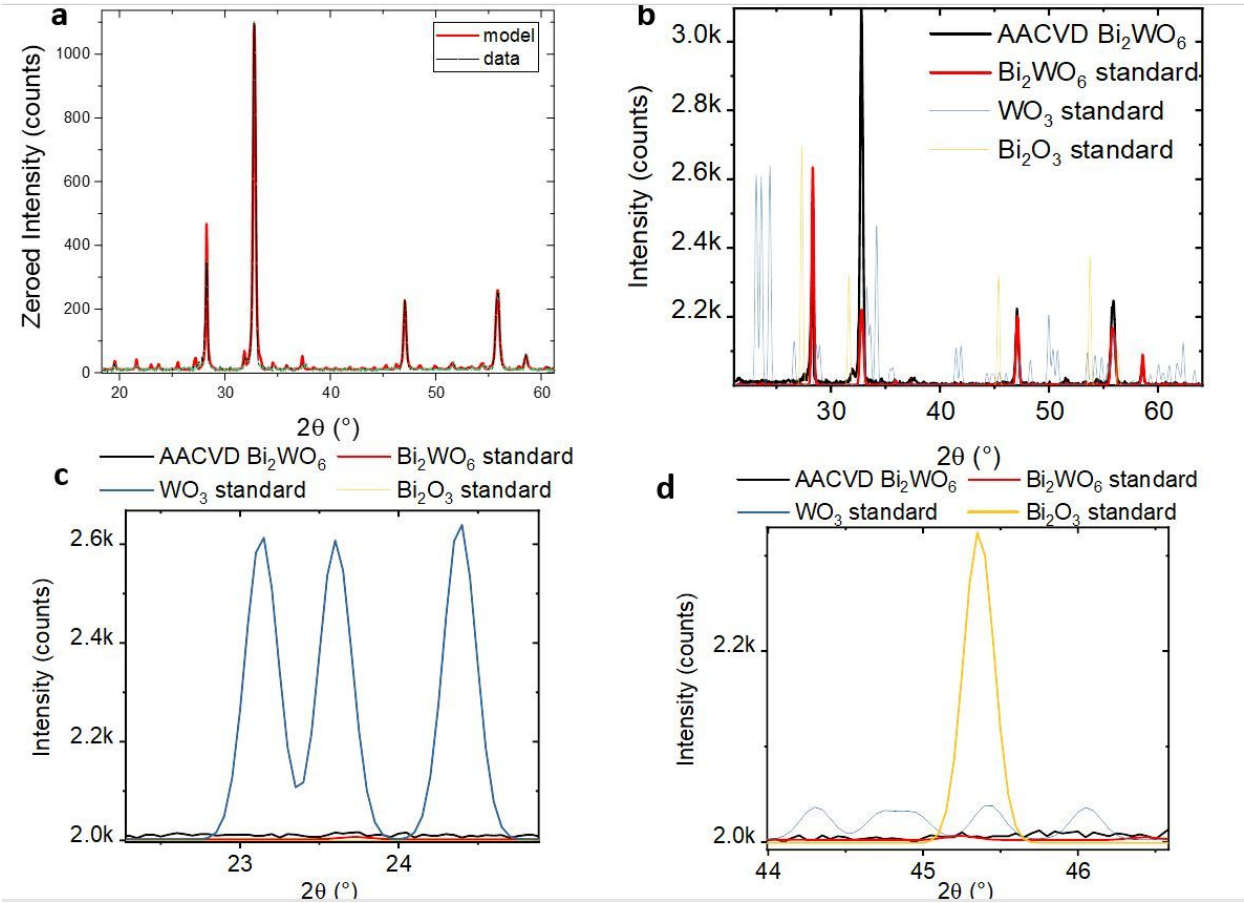


*Figure S0. (a) Measured and modelled diffraction patterns of AACVD $Bi_2WO_6$ (b) magnified comparison of AACVD $Bi_2WO_6$ in comparison to standards for $WO_3$ and $Bi_2O_3$. (c) and (d) show magnified regions of (b).*

## S1. XPS

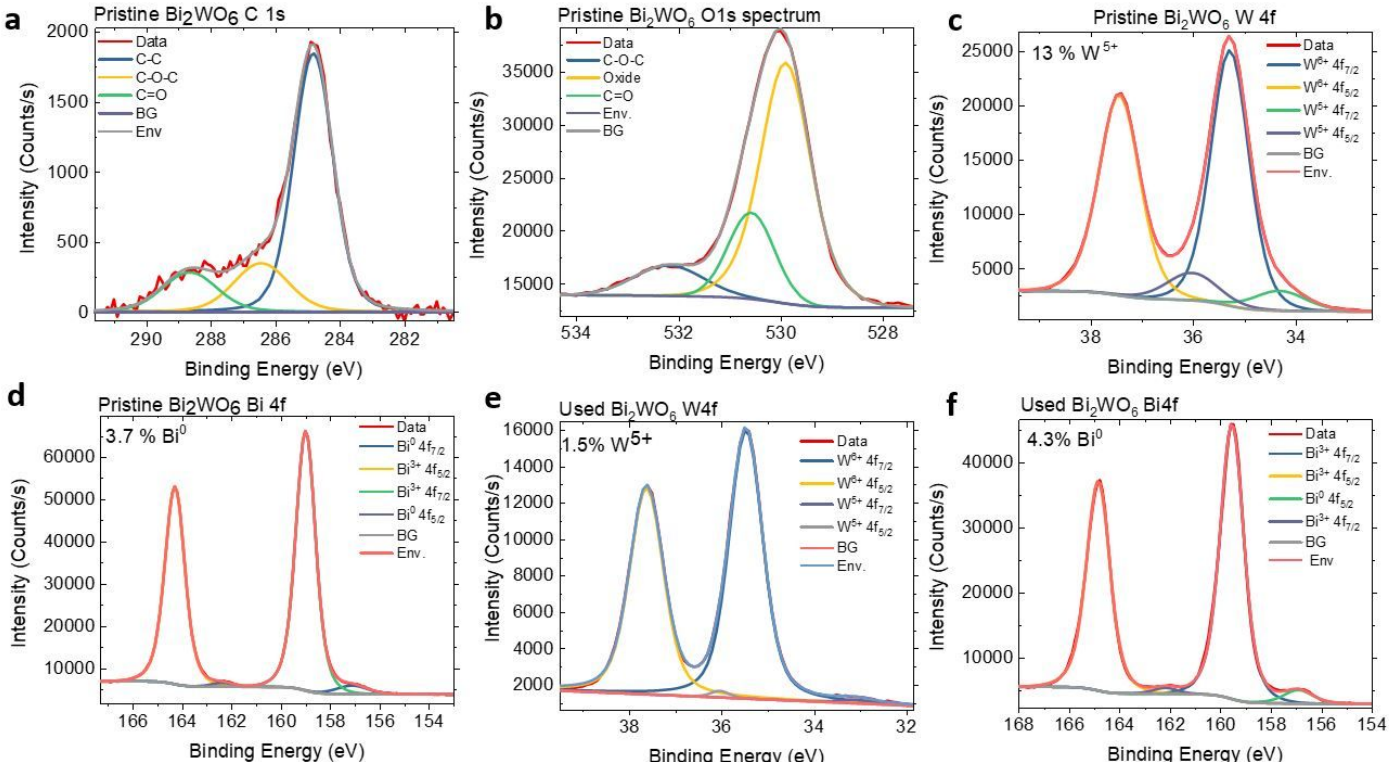


**Figure S1.** C 1s (a) O1s (b) W 4f (c) Bi 4f (d) photoemission spectra of pristine $Bi_2WO_6$. W 4f (e) and Bi 4f (f) spectra of used $Bi_2WO_6$

Figure S1 shows C 1s, O 1s, W 4f and Bi 4f of pristine $Bi_2WO_6$. The C 1s spectrum (S1a) show three adventitious C environments typical of (C-C), (C-O) and (C=O).[1] Two adventitious oxygen environments (S1b) are observed arising from adventitious carbon residues, with a larger peak attributable to $O^{2-}$ anions in the lattice.[2] The W 4f spectrum (S1c) shows two doublets, attributable to $W^{6+}$ and $W^{5+}$ respectively. This has previously been attributed the presence of oxygen deficiency leading to the reduction of $W^{6+}$ states.[3] A remarkably high $W^{5+}$ concentration of 13 % is observed. The Bi 4f spectrum also shows two distinct environments (S1d), which we attribute to $Bi^{3+}$ and $Bi^{0}$ states. During the first few minutes of use, a drop in oxidative photocurrent is observed before steady water oxidation current is observed (see stability test, S6). This effect is observed only once and appears to be irreversible, as oxidation of $W^{5+}$ states are observed in used samples – with a $W^{5+}$ concentration nearly 10 times lower than in the pristine samples (S1e). In contrast the $Bi^{0}$ concentration appears to be unaffected by use (S1f).

## S2 Cross sectional SEM

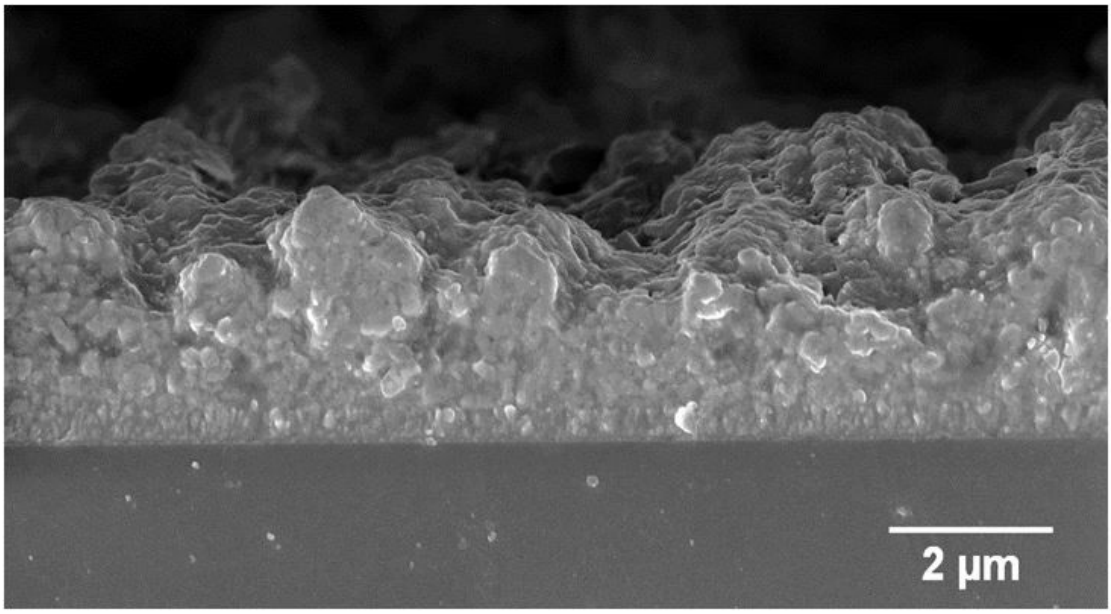


***Figure S1.*** Cross-sectional SEM image of a typical $Bi_2WO_6$ film.

## S3 EDX of $Bi_2WO_6$

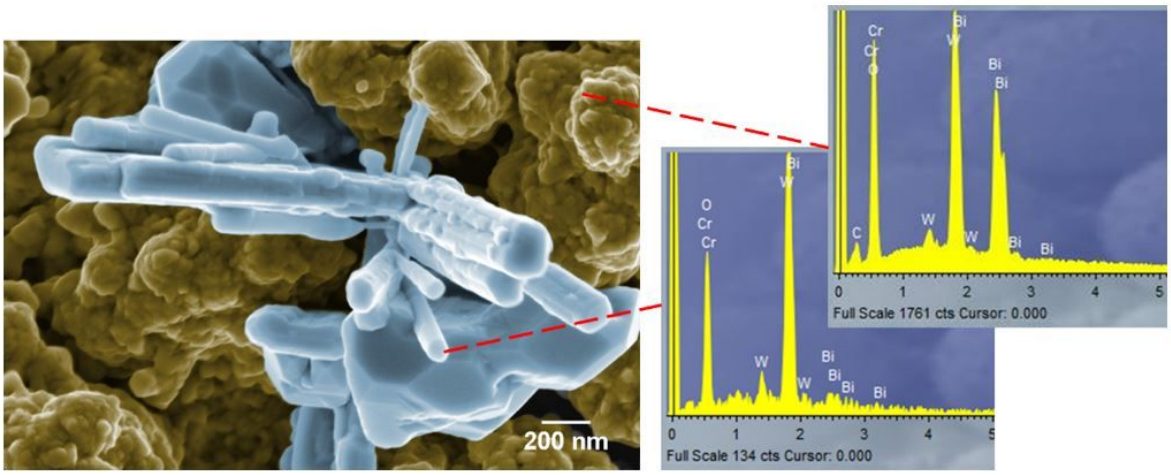


**Figure S2** EDX image of a nanoscale $WO_3$ impurity (< 1%) in comparison to the $Bi_2WO_6$ film

**S4 High magnification images SEM of $Bi_2WO_6$**

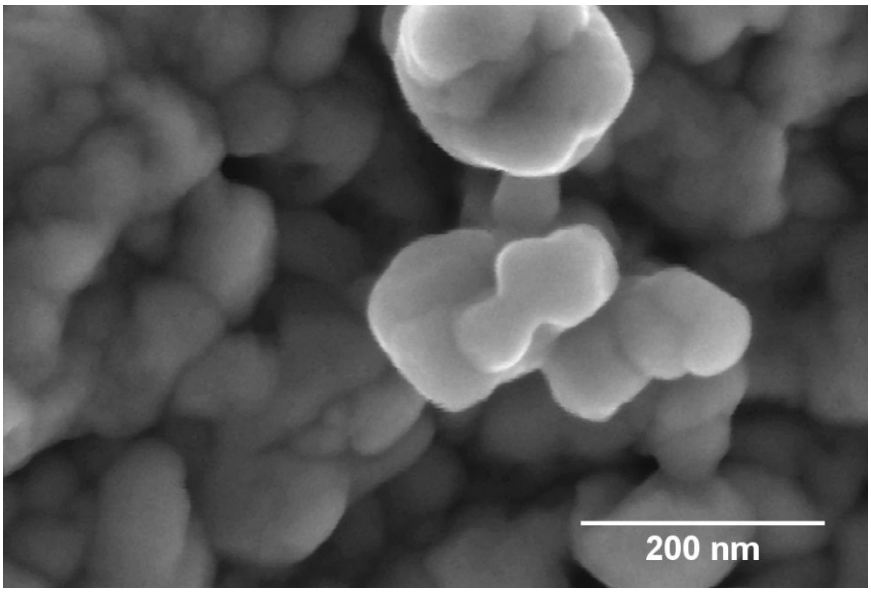


**Figure S3**. High magnification SEM image of typical $Bi_2WO_6$ film.

**S5 Reflectance spectrum of $Bi_2WO_6$**

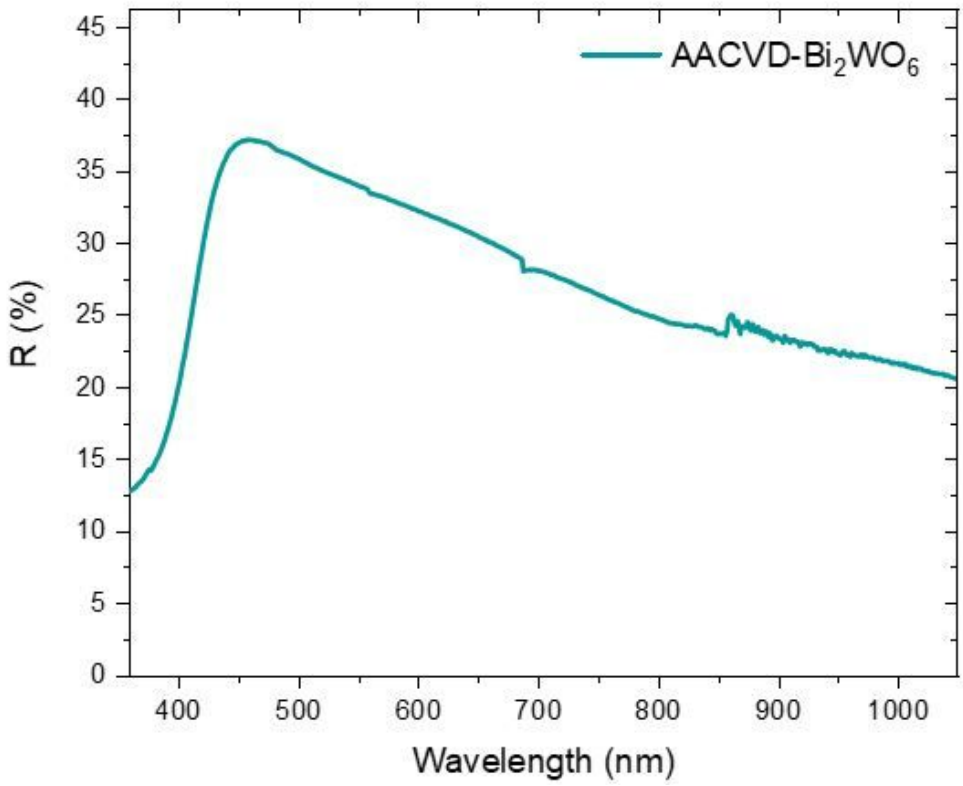


**Figure S5.** Diffuse reflectance spectrum of $Bi_2WO_6$

**S6 Photoelectrochemical stability of $Bi_2WO_6$**

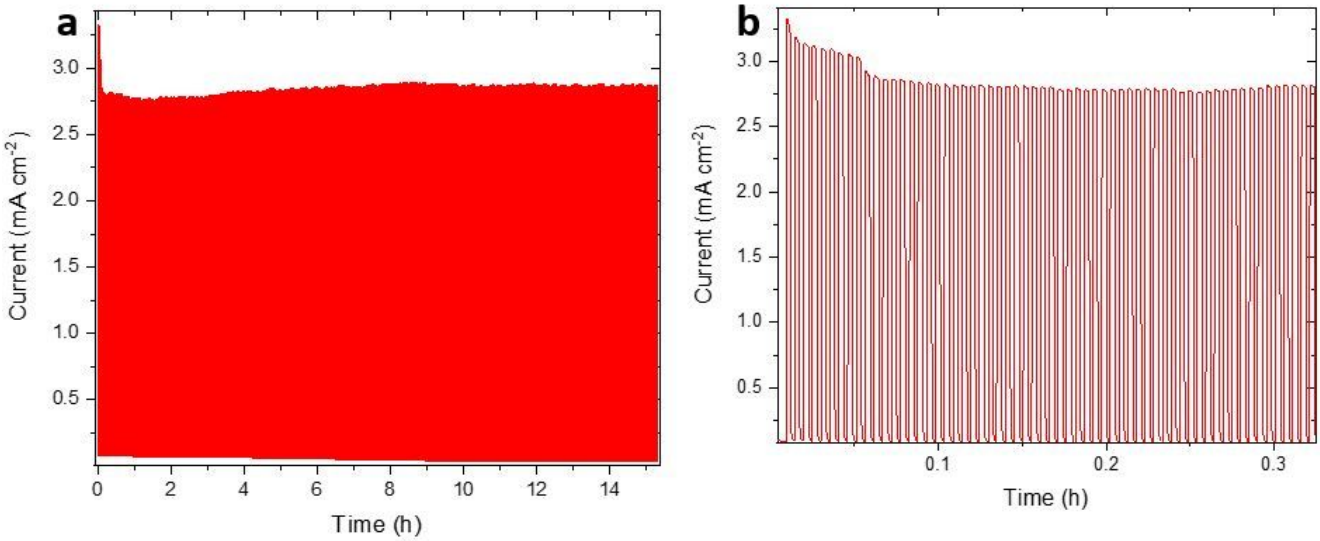


***Figure S6.*** Photoelectrochemical chopped light stability test for a $Bi_2WO_6$ photoanodes. (a) LED illumination was chopped for the 15 hours. (b) The first 20 minutes of the stability test. Conditions: 0.1 M phosphate buffer (pH = 7) at 1.23 $V_{RHE}$ under chopped light irradiation (375 nm; ~7.5 mW.cm$^{-2}$).

Figure S6 shows the results of photoelectrochemical stability testing of $Bi_2WO_6$ using a high intensity UV LED. A c.a. 19 % drop in photocurrent is observed within the first few minutes of continuous light chopping, after which stable photocurrent is observed for over 14 hours. We attribute this loss to the initial oxidation of reduced $W^{5+}$ states in the material.

**Table S1**: *Summary of the synthesis, structure and key performance parameters towards photoelectrochemical water splitting for $Bi_2WO_6$ photoanodes in the literature.*

| Synthesis | Structure | Onset† | Photocurrent‡ | Stability§ | Reference |
|---|---|---|---|---|---|
| **Sol-gel** | Nanoscale Inverse opals | ~0.7 | ~0.12* | ~7%; ~1200 mins | Bahnemann *et al.*[4,5] |
| **Electrochemical and solid-state** | Micron-sized mesopores | ~0.7 | ~0.30 | ~50%; ~10 mins | Choi *et al.*[6] |
| **Hydrothermal** | Vertical nanoplates | ~0.5 | ~0.22 | ~5%; ~3 mins | Bi *et al.*[7] |
| **Drop-casting** | Nanoporous | ~0.3 | ~0.12 | ~18%; ~7 mins | Bi *et al.*[8] |
| **Solvothermal** | Bi-pyramidal nanostructure | *nm* | ~0.020 | ~30%; ~3 mins | Li *et al.*[9] |
| **Hydrothermal** | Nano-needle structures | ~0.3 | ~0.012 | *nm* | Joo *et al.*[10] |
| **AACVD** | Micron-sized mounds | ~0.5 | ~0.17 | ~19%; ~900 mins | herein |

†onset potential of photocatalytic water oxidation ($V_{RHE}$); ‡photocurrent at 1.23 $V_{RHE}$ and 1 sun irradiance (mA.cm$^{-2}$); §the photocurrent drop (%) after a given time (mins);*15% of 1 sun irradiance in terms of power; *nm* = not measured.

**S7 Ultra-fast transient absorption kinetics.**

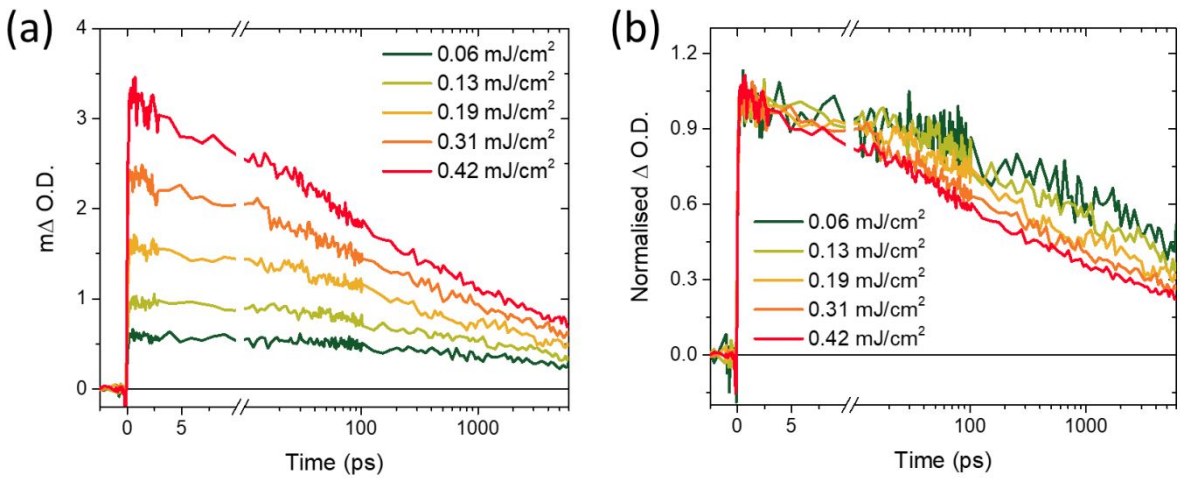


**Figure S7.** Power dependence of ultra-fast recombination kinetics in $Bi_2WO_6$ under an inert atmosphere at 600 nm.

**Table S2.** Comparison of transient recombination 50% decay times under an inert atmosphere

| **Material** | **$t_{50\%}$ (from 1 ps)** | **$T_{50\%}$ (from 1 us)** | **Reference** |
|---|---|---|---|
| **$TiO_2$** | 1000-2000 | 100 | [11,12] |
| **$Fe_2O_3$** | 10-30 | 10 | [11,13] |
| **$WO_3$** | 6-30 | 100 | [14,15] |
| **$BiVO_4$** | 15-80 | 200 | [16] and S8 |
| **$Bi_2WO_6$** | 200-2000 | 100 | This work |

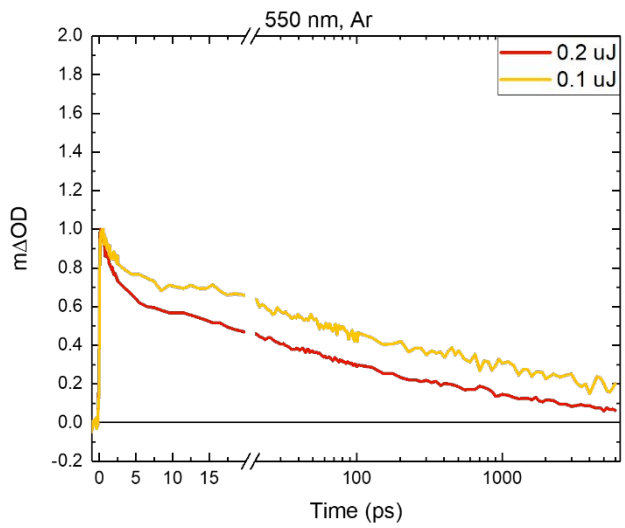


**Figure S8**. Ultra fast recombination kinetics of $BiVO_4$ under an inert atmosphere. Included to complete the dataset in Table S2

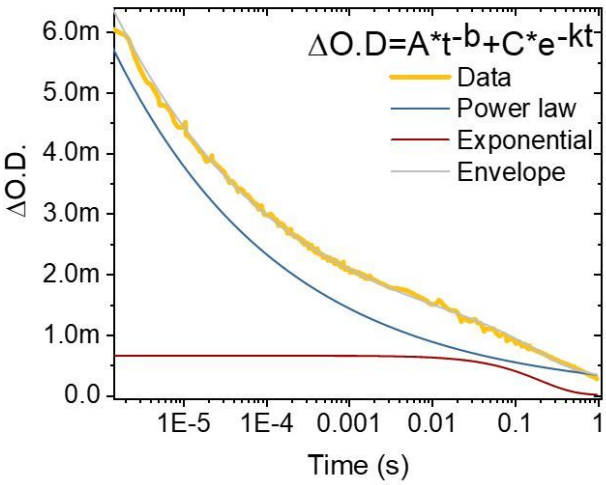


| Applied Potential (V vs RHE) | A | B | C | k | average k |
|---|---|---|---|---|---|
| 0.3 | 0.000132 | 0.28536 | 9.16E-05 | 4.9997 | 7.23 |
| 0.5 | 0.00017 | 0.27131 | 0.0001 | 9.9998 | |
| 1 | 0.000149 | 0.27844 | 0.0004 | 10 | |
| 1.5 | 0.000171 | 0.26365 | 0.000618 | 8.8607 | |
| 2 | 0.000241 | 0.23526 | 0.000724 | 5.885 | |
| 2.5 | 0.000231 | 0.23762 | 0.0009 | 3.688 | |

**Figure S9**. Example of a transient decay fitted to the sum of a power law and exponential decay functions shown alongside the final parameters resulted from fitting the transients in Figure 2c.

## S10 Correlation of photocurrent and exponential transient absorption amplitude

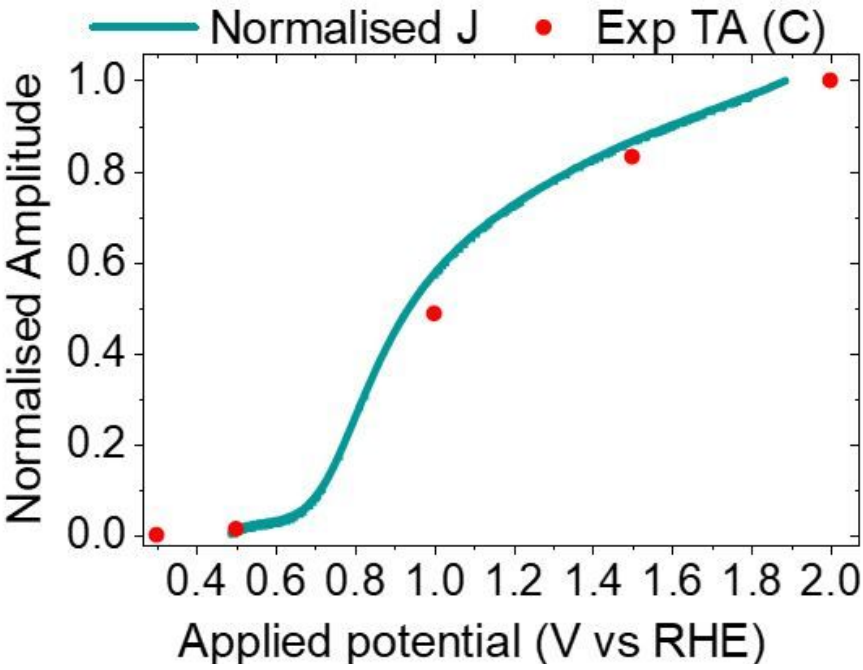


**Figure S10.** Correlation of normalised amplitude of the exponential transient absorption component (C in Fig. S9) against photocurrent.

## S11 Analysis of crystal growth.

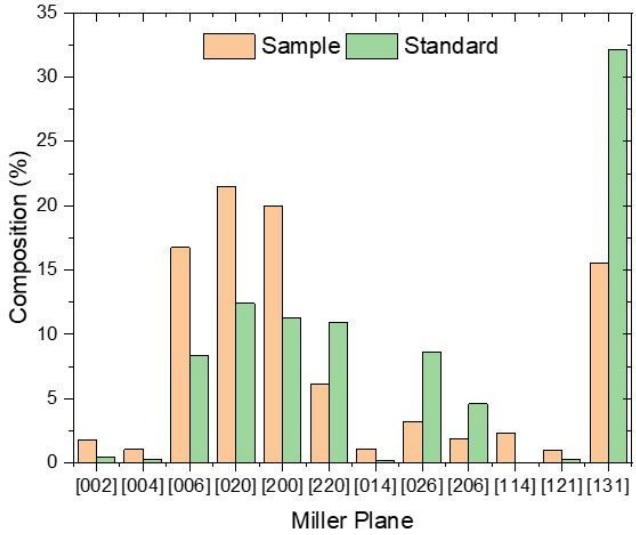


**Figure S11.** Comparison of predominant miller planes in $Bi_2WO_6$ to a crystallographic standard (note: the long axis of the unit cell is defined as the b axis herein).

(1) Gelius, U.; Hedén, P. F.; Hedman, J.; Lindberg, B. J.; Manne, R.; Nordberg, R.; Nordling, C.; Siegbahn, K. Molecular Spectroscopy by Means of ESCA III. Carbon Compounds. *Phys. Scr. 2* (1–2), 70–80.

(2) Dupin, J.-C.; Gonbeau, D.; Vinatier, P.; Levasseur, A. Systematic XPS Studies of Metal Oxides , Hydroxides and Peroxides. *Phys. Chem. Chem. Phys.* **2000**, *2* (6), 1319–1324.

(3) Corby, S.; Francàs, L.; Selim, S.; Sachs, M.; Blackman, C.; Kafizas, A.; Durrant, J. R. Water Oxidation and Electron Extraction Kinetics in Nanostructured Tungsten Trioxide Photoanodes. *J. Am. Chem. Soc.* **2018**, *140* (47), 16168–16177.

(4) Zhang, L.; Bahnemann, D. Synthesis of Nanovoid Bi2WO6 2D Ordered Arrays as Photoanodes for Photoelectrochemical Water Splitting. *ChemSusChem* **2013**, *6* (2), 283–290.

(5) Zhang, L.; Baumanis, C.; Robben, L.; Kandiel, T.; Bahnemann, D. Bi 2WO 6 Inverse Opals: Facile Fabrication and Efficient Visible-Light-Driven Photocatalytic and Photoelectrochemical Water-Splitting Activity. *Small* **2011**, *7* (19), 2714–2720.

(6) Hill, J. C.; Choi, K. S. Synthesis and Characterization of High Surface Area CuWO4 and Bi2WO6 Electrodes for Use as Photoanodes for Solar Water Oxidation. *J. Mater. Chem. A* **2013**, *1* (16), 5006–5014.

(7) Dong, G.; Zhang, Y.; Bi, Y. The Synergistic Effect of Bi 2 WO 6 Nanoplates and Co 3 O 4 Cocatalysts for Enhanced Photoelectrochemical Properties. *J. Mater. Chem. A* **2017**, *5* (39), 20594–20597.

(8) Dong, G.; Zhang, Y.; Wang, W.; Wang, L.; Bi, Y. Facile Fabrication of Nanoporous Bi 2 WO 6 Photoanodes for Efficient Solar Water Splitting. *Energy Technol.* **2017**, *5* (11), 1912–1918.

(9) Zhang, G.; Hu, Z.; Sun, M.; Liu, Y.; Liu, L.; Liu, H.; Huang, C. P.; Qu, J.; Li, J. Formation of Bi2WO6 Bipyramids with Vacancy Pairs for Enhanced Solar-Driven Photoactivity. *Adv. Funct. Mater.* **2015**, *25* (24), 3726–3734.

(10) Chae, S. Y.; Lee, E. S.; Jung, H.; Hwang, Y. J.; Joo, O. S. Synthesis of Bi2WO6 Photoanode on Transparent Conducting Oxide Substrate with Low Onset Potential for Solar Water Splitting. *RSC Adv.* **2014**, *4* (46), 24032–24037.

(11) Pendlebury, S. R.; Wang, X.; Le Formal, F.; Cornuz, M.; Kafizas, A.; Tilley, S. D.; Grätzel, M.; Durrant, J. R. Ultrafast Charge Carrier Recombination and Trapping in Hematite Photoanodes under Applied Bias. *J. Am. Chem. Soc.* **2014**, *136* (28), 9854–9857.

(12) Cowan, A. J.; Leng, W.; Barnes, P. R. F.; Klug, D. R.; Durrant, J. R. Charge Carrier Separation in Nanostructured TiO2 Photoelectrodes for Water Splitting. *Phys. Chem. Chem. Phys.* **2013**, *15* (22), 8772–8778.

(13) Barroso, M.; Mesa, C. A.; Pendlebury, S. R.; Cowan, A. J.; Hisatomi, T.; Sivula, K.; Graẗzel, M.; Klug, D. R.; Durrant, J. R. Dynamics of Photogenerated Holes in Surface Modified α-Fe 2O3 Photoanodes for Solar Water Splitting. *Proc. Natl. Acad. Sci. U. S. A.* **2012**, *109* (39), 15640–15645.

(14) Sachs, M.; Park, J. S.; Pastor, E.; Kafizas, A.; Wilson, A. A.; Francàs, L.; Gul, S.; Ling, M.; Blackman, C.; Yano, J.; Walsh, A.; Durrant, J. R. Effect of Oxygen Deficiency on the Excited State Kinetics of WO3 and Implications for Photocatalysis. *Chem. Sci.* **2019**, *10* (22), 5667–5677.

(15) Corby, S.; Francàs, L.; Kafizas, A.; Durrant, J. R. Determining the Role of Oxygen Vacancies in

the Photoelectrocatalytic Performance of WO3 for Water Oxidation. *Chem. Sci.* **2020**, *11* (11), 2907–2914.

(16) Ma, Y.; Pendlebury, S. R.; Reynal, A.; Le Formal, F.; Durrant, J. R. Dynamics of Photogenerated Holes in Undoped BiVO4 Photoanodes for Solar Water Oxidation. *Chem. Sci.* **2014**, *5* (8), 2964–2973.